Murshed H. Al-Janabi [1]
Çiğdem Y. Ataol [1]
Asmiet Ramizy [2]

[1] *Department of Physics, Faculty of Science, Çankırı Karatekin University, 18100, Çankırı, TURKEY*
[2] *Department of Physics, College of Science, University of Anbar, Ramadi, IRAQ*

Characterization of Silver Nanoparticles Prepared by Cold Plasma Reaction

In this study, varied exposure period of an atmospheric pressure non-thermal plasma technique were used to prepare silver nanoparticles (Ag NPs). The structural, morphological and spectroscopic characteristics of the Ag nanoparticles were examined. Surface plasmon resonance (SPR) centers at 416, 417, 421, 428 and 433nm were observed in the synthesized Ag nanoparticles. These nanoparticles were face-centered cubic crystals with crystalline composition. The average crystallite size of the Ag nanoparticles was 30.9 nm. Additionally, the formation of spherical Ag particles with sizes within 17-55nm was confirmed. The plasma exposure period, according to the results, is a key factor in changing the attributes of silver nanoparticles such as surface area, grain size, and optical stability. The well diffusion method and the MIC method were used to examine the biological activity of synthetic Ag nanoparticles against various harmful bacteria (Staphylococcus aureus, E. coli). When using the well diffusion approach to combat both Gram-positive and Gram-negative bacteria, the Ag nanoparticles demonstrated greater antibacterial activity.

Keywords: Cold Plasma; Nanoparticles; Silver; Thin Films
Received: 04 November; **Revised:** 05 December; **Accepted:** 12 December 2023

1. Introduction

Interest in nanoscience and nanotechnology has grown recently as a result of the global focus on research and development in these fields [1,2]. Due to their unique properties, nanoparticles can be used for a wide variety of practical uses considering characteristics such as size, shape, distribution, and a large surface area to volume ratio [3,4]. Metallic nanoparticles have been employed in a variety of applications, including conductive pastes, optoelectronics, fuel cells, catalysis, magnetics, microelectronics, conductive pastes, and battery electrodes [5,6]. Metallic nanoparticles have unique properties that set them distinct from bulk materials because of the quantum size effect [7,8].

According to the ASTM standard definition, nanoparticles are two- or three-dimensional particles having lengths between 1 and 100 nm [9]. Nanoparticles display new or fully optimized characteristics, such as molecule size, distribution, and morphology. Due to their increased surface area relative to weight or volume and distinct physical, biological, and chemical characteristics compared to bulk material, nanoscale particles are highly unusual in nature [10]. Among the diverse nanomaterials available, noble metallic nanoparticles have been used in a variety of applications in the fields of electronic, magnetic, optoelectronics, and information storage [11]. The noble metal nanoparticles category includes silver nanoparticles (Ag NPs), which have received substantial research due to their outstanding physical, chemical, and biological properties. Their superiority stems mostly from the shape, size, crystallinity, composition, and structure of Ag nanoparticles as compared to their bulk forms [12]. At present, nanoparticles of silver (Ag) and gold (Au) are utilized in a variety of biomedical, antibacterial, and anti-cancer treatments, drug transport, entomological, catalysis, anti-biofilm, agriculture antioxidant, anti-fungal and parasitological applications [13].

Using plasma systems to synthesize nanoparticles or green synthesis has made it possible to produce nanoparticles at a faster rate and a lower cost than ever before. Some examples of these are micro plasma reduction, arc in water, laser-induced plasma, glow discharge, and glow discharge processes [14]. Rapid and chemical-free production of metal nanoparticles is possible in plasma systems. Plasma is a powerful catalyst due to the extremely excited energy levels it generates in the reaction field. In this process, an electron acts as the reducing agent. Plasmas produced in or near liquids have been shown to produce metal nanoparticles. [15]. While the ions and molecules (and thus the gas as a whole) remain at almost their original temperatures, the applied electric field heats free electrons to several electron-volts (eV), which is enough to ionize them and trigger chemical processes in cold or non-equilibrium plasma. When plasma is cold or out of balance, its catalytic properties allow it to activate several processes and speed up reaction times [16].

2. Experimental Part

In order to synthesize silver nanoparticles (Ag NPs) by atmospheric pressure plasma jet, aqueous solutions of silver nitrate ($AgNO_3$) were prepared in concentrations of 0.6, 0.8, 1, 1.2, 1.4 mM and plasma exposure time of 4 min. As a stabilizing agent, the mixture was amended with fructose. At a concentration of 0.001 M and mixed with the $AgNO_3$ solution. The experiment consists of a hole metal tube

of stainless steel with an inner diameter of 1 mm and length of 3 cm that connect to the cathode of a high voltage dc power supply. A small volume (10 ml) of prepared solution ($AgNO_3$) was put in a beaker. The beaker was placed upon the movement stage under the tube, and the gap between the stainless tube's tip and the solution's surface was kept at 1 cm. A square piece of stainless-steel foil (dimensions of 1x1cm) was immersed attached to the anode of the power supply and dissolved in the prepared solution. The stainless tube was connected to the argon gas through a flowmeter the flow of gas was adjusted to 2 Ltr/min and the discharge voltage was 6 kV. Figure (1) shows a photograph of the experimental setup.

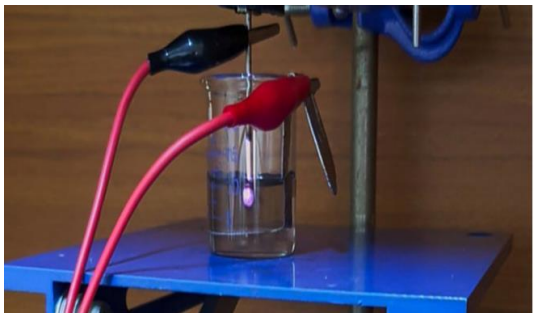

Fig. (1) Cold plasma experimental setup in liquid

The plasma was generated between the stainless tube and surface solution after switching on the circuit. Initially, the color of the $AgNO_3$ solutions was transparent and it varied to a dark brown after a few minutes of the treatment with plasma, which indicate the formation of Ag nanoparticles. The synthesized nanoparticles were characterized using Zeiss Ultra Plus field-emission electron microscope (FE-SEM), Shimadzu, UV-3600 UV-Visible spectrometers, and Philips PW 1710 x-ray diffractometer system.

3. Results and Discussion

A cold plasma system was used to produce silver nanoparticles. The color change is an early indicator of the formation of Ag nanoparticles. The absorption spectra of Ag nanoparticles is clarified in Fig. (2) where the absorption peaks appear at 416, 417, 421, 428 and 433 nm for $AgNO_3$ concentrations of 0.6, 0.8, 1, 1.2 and 1.4 mM, respectively, at 4 minutes of plasma exposure. The $AgNO_3$ solution's color changed from translucent to dark brown, suggesting the emergence of Ag nanoparticles, because of the peak shifted to red due to the surface plasmon resonance (SPR) of Ag nanoparticles where SPR occurs in specific metals such as silver and gold because of the arrival of its particle diameter to the nanoscale [17,18]. The observed variation in the absorption peak intensity with plasma treatment time shows that this method of producing silver nanoparticles was successful; the variation in the absorption regions is caused by the nanosilver, whereas the variation in the altitude peaks is caused by the concentration of nanosilver in the solution. The interactions between free electrons contained inside silver nanoparticles and plasma exposure produce absorption spectra [19,20].

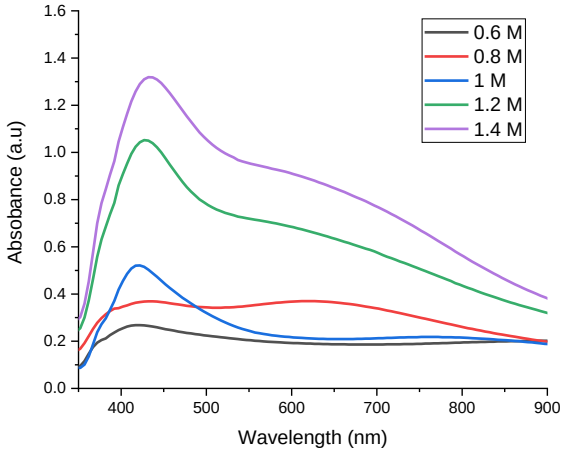

Fig. (2) UV-Visible absorption spectra of Ag NPs prepared using different concentrations of $AgNO_3$ (0.6, 0.8, 1, 1.2, and 1.4 mM) at 4 min. of plasma exposure

The x-ray diffraction (XRD) patterns shown in Fig. (3) belong to prepared silver nanoparticles as a function of $AgNO_3$ solution concentration (0.6, 0.8, 1, 1.2, and 1.4 mM) with plasma exposure time of 4 minutes on silicon substrate.

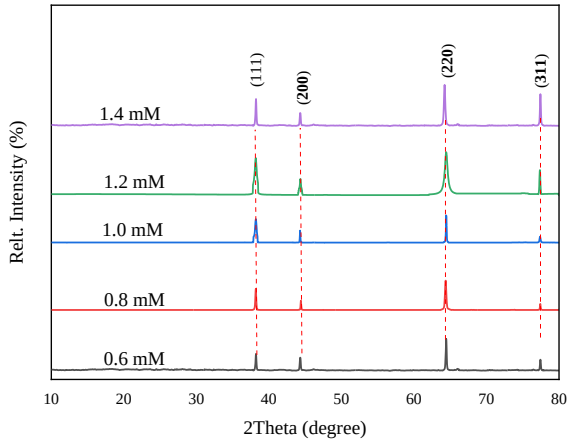

Fig. (3) XRD patterns of Ag nanoparticles prepared with different concentrations of $AgNO_3$ solution (0.6, 0.8, 1, 1.2, and 1.4 mM) at 4 min. of plasma exposure

By comparing the results with the standard cards (JCPDS card 04-0783), it was found that the thin films have cubic structure, with the appearance of crystalline levels (111), (200), (220), and (311) at the diffraction angles of 38.1°, 44.27°, 64.4°, and 77.4°, respectively. These peaks agreed well with the cubic structure of the space group (JCPDS card 04-0783), referring that the crystalline growth of Ag nanostructures at different concentrations being in the same cubic phase. The increase in $AgNO_3$ solution concentration led to a high degree of crystallinity of prepared silver nanoparticles and the broad peaks indicate the formation of nanoparticles. The high peak observed at 28.4° is attributed to the silicon

substrate. At a higher concentration (1.4 mM), an increase in the peak intensity indicates high crystallization of the $AgNO_3$ phase, which is attributed to the high concentration of $AgNO_3$ in the starting solution [21,22].

The FE-SEM images of Ag nanoparticles prepared with different $AgNO_3$ solution concentrations (0.6, 0.8, 1, 1.2, and 1.4 mM) are shown in Fig. (4) at a plasma exposure time of 4 min. These images showed that when the concentration of $AgNO_3$ is increased, the particle size of the prepared Ag nanoparticles reduced, and the average particle sizes are 63.8, 45.13, 44.16, 38.11, and 26.05 nm for the $AgNO_3$ concentrations of 0.6, 0.8, 1, 1.2, and 1.4 mM), respectively, with almost spherical shape.

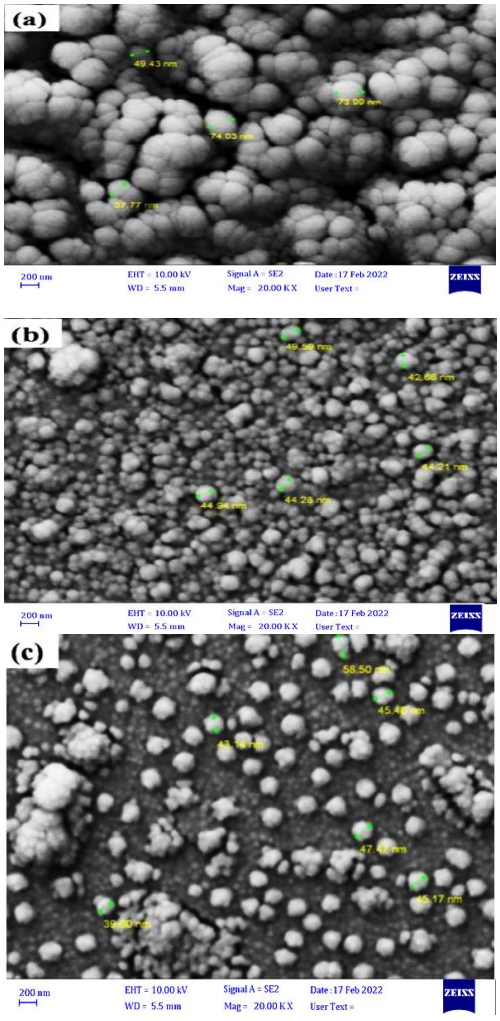

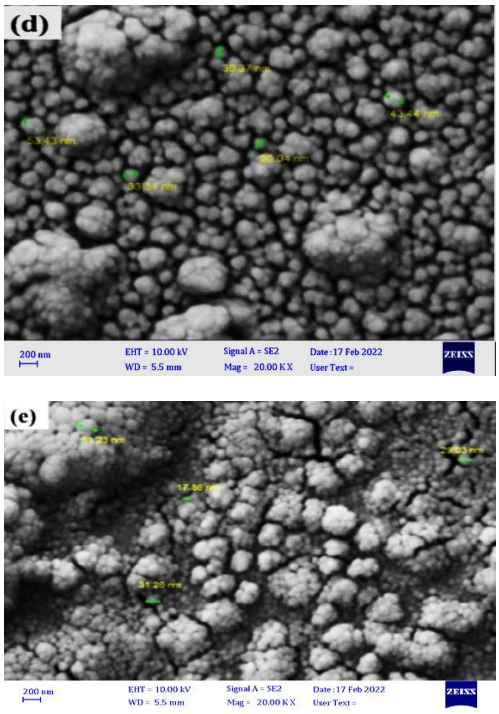

Fig. (4) FE-SEM images of Ag nanoparticles prepared with different concentrations of $AgNO_3$ (a) 0.6 mM, (b) 0.8 mM, (c) 1 mM, (d) 1.2, (e) 1.4 mM, at plasma exposure time of 4 min

There was a small amount of non-spherical silver nanoparticles which are usually detected in plasma-assisted synthesis technique. With the increase of $AgNO_3$ concentration as more silver nanoparticles were produced, the concentration of the ionic silver precursor steadily decreased. When the concentration of the silver precursor is low, anisotropic growth of the produced silver nanoparticles is favored to nucleation of new nanoparticles [23].

Most often, semi-elastic light scattering is associated with dynamic light scattering. The dynamic light scattering (DLS) is used to assess the dispersion and size of nanoparticles because it controls the size distribution and selective aggregation of nanoparticles [23]. The silver nitrate nanoparticle solution obtained after 4 min plasma discharge for different initial $AgNO_3$ concentrations (0.6, 0.8, 1, 1.2, and 1.4 mM) is analyzed by DLS for particle size determination. In Fig. (5), the particles produced by the plasma flow method during a 4-minute treatment period at a concentration of 0.6 mM had a single size that indicated 100% of the particles had a diameter of 54.96 nm, and the particle diameter is ranging between 34 and 147 nm. The DLS results shown in Fig. (5a) present the size distribution of the particles of the concentration 1 mM, indicating that 100% of the particles have a diameter of 91.48 nm and that particle diameter values are ranging between 45 and 220 nm. Figure (5b) shows the size distribution of the particles prepared with $AgNO_3$ concentration of 0.8 mM.

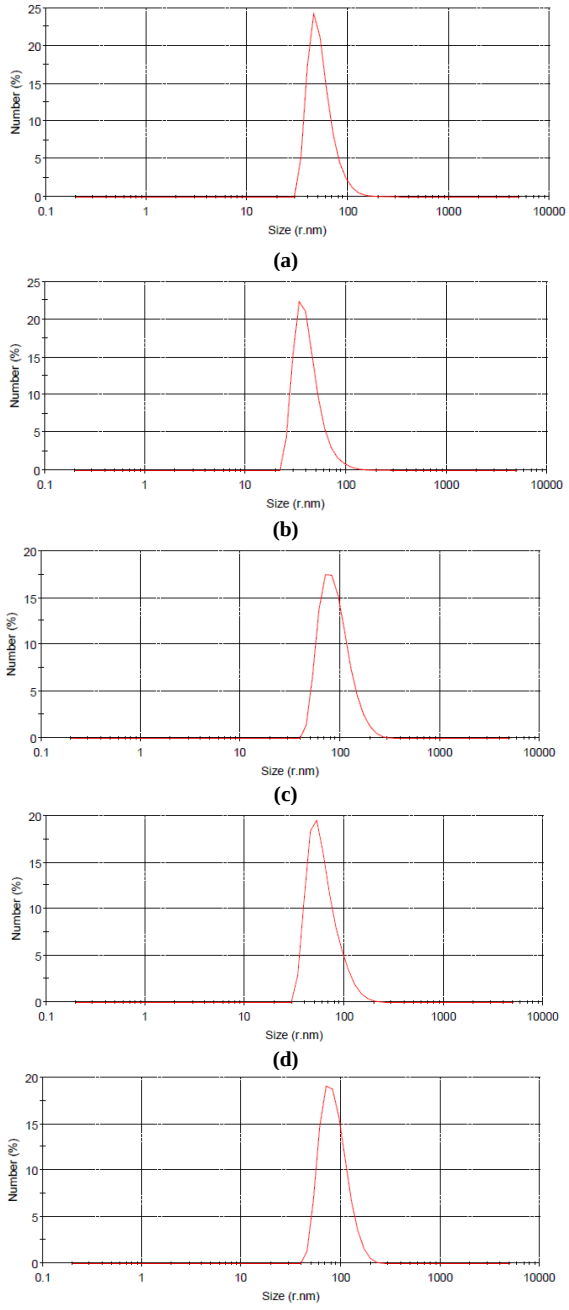

Fig. (5) Particle size distribution of the sample prepared with concentration of (a) 0.6 mM, (b) 0.8 mM, (c) 1 mM, (d) 1.2 mM, and (e) 1.4 mM

The findings of the DLS show that 100% of the particles have a diameter of 42.81 nm in the range of 30-127 nm, demonstrating that the range of particle diameters is between 45 and 200 nm and that all of the particles have a diameter of 87.25 nm. It is important to be aware that the polydispersity index (PDI) for DLS is computed by $(\text{width/mean})^2$ for each peak and generally illustrates the intensity of light dispersed by different percentages of particles of different sizes. While values of PDI between 0.1 and 0.4 and higher are thought to be moderately and extremely polydisperse, respectively, PDI 0.1 is thought to be very monodisperse [23].

Zeta potential measurements may also be used to evaluate the stability of colloidal particles. Absolute values are used to depict the electrical charge on the surface of the particle. When a substance's zeta potential falls between 0 and 10 mV, 10 and 20 mV, 20 and 30 mV, and 30 mV, it is said to be very unstable, reasonably stable, moderately stable, or highly stable, respectively [24]. In the current study, the results of Ag nanoparticles were obtained after 4 min plasma discharge for different initial $AgNO_3$ concentrations (0.6, 0.8, 1, 1.2, and 1.4 mM), as shown in Fig. (6).

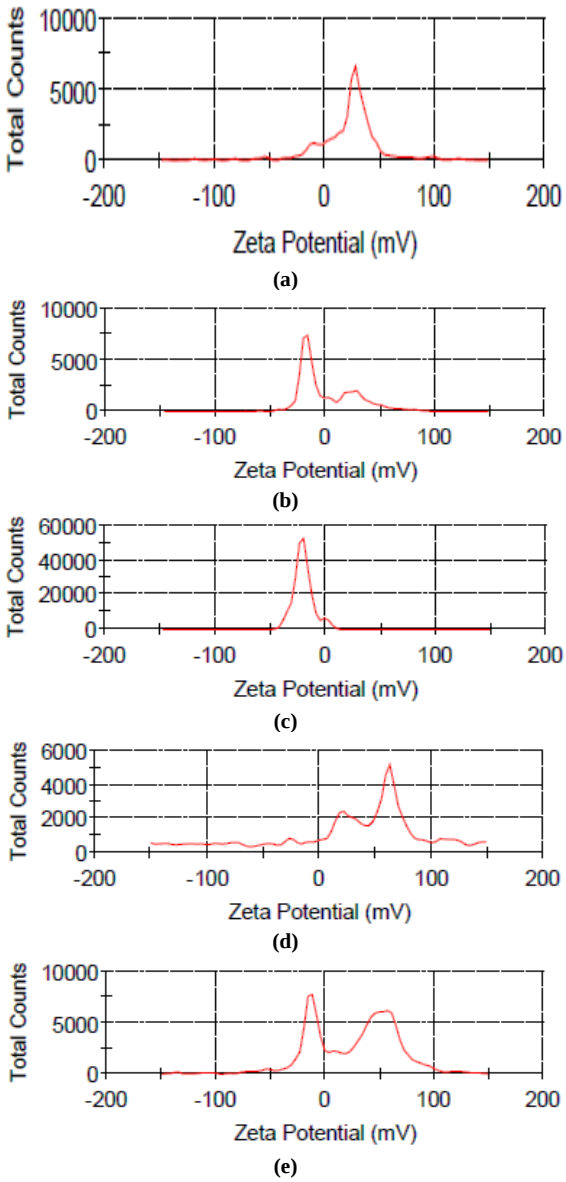

Fig. (6) Zeta potential measurement of the sample prepared with concentration of (a) 0.6 mM, (b) 0.8 mM, (c) 1 mM, (d) 1.2 mM, and (e) 1.4 mM

The Z-potential value of the concentration 0.6 mM was found to be 27.2 mV in Fig. (6a), while the Z-potential with a concentration 0.8 mM was -16 mV as illustrated in Fig. (6b). Also, the Z-potential value of concentration 1 mM was found to be -21.3 mV, as shown in Fig. (6c), and the Z-potential value of

concentration 1.2 mM was found to be 65.5 mV, as shown in Fig. (6d). Finally, the Z-potential value of the concentration 1.4 mM was found to be 40.2 mV, as shown in Fig. (6e), and that is due to the high aggregation that occurs in this concentration.

A mass spectrometer that is inductively linked to plasma was used to find the additional impurities contained in the liquid as well as the dissolved metal components of $AgNO_3$. The ICP-MS is an analytical method used to qualitatively and quantitatively assess components in solution or liquid samples. ICP-MS analysis offers data on elemental abundance at extremely high precision (parts per billion), which is useful for testing heavy elements in particular [25]. Since the maximum percentage was at concentration, the results indicated that the concentration of silver nanoparticles increased as 1mM of $AgNO_3$ concentration is increased (see table 3). Additionally, the samples' ICP-MS analysis revealed that the technique allowed for effective ionization and identification of the metal impurities that are frequently found in silver nitrate precursors, such as Al, Se, Te, Ni, Zn, P, etc.

Table (3) Results of ZOI by Well Diffusion Method of Ag NPs, against (Escherichia coli, Staphylococcus aureus)

Concentration (mM)	Staphylococcus aureus	Escherichia coli
0.6	15.43427	12.56828
0.8	14.32116	12.91816
1	15.01592	13.73081
1.2	14.1871	13.68434
1.4	15.47548	14.32116

4. Conclusions

In the proposed work, non-thermal air plasma was used to produce Ag nanoparticles. Ag nanoparticles' absorption spectrum peaks, which are indicative of noble metal nanoparticles, were discovered to be in the (390–420 nm) range when they were subjected to UV-VIS spectroscopic analysis. X-ray diffraction proved Ag nanoparticles were present. For Ag nanoparticles, it was discovered to contain four distinct peaks of 2 at 38.1°, as well as peaks at 44.27°, 64.42°, and 77.47°. The FE-SEM topographies showed that when the quantity of $AgNO_3$ grew, the produced Ag nanoparticles' particle size increased as well. This study's nanoparticles were found to have antibacterial activity against both Gram-positive (Staphylococcus aureus) and Gram-negative (Escherichia coli) bacteria, which was found to be very encouraging evidence that these nanoparticles were also effective against other types of pathogenic bacteria.

References

[1] B. Bhushan, (ed.), **"Springer Handbook of Nanotechnology"**, Springer (2017).

[2] G.L. Hornyak et al., **"Fundamentals of Nanotechnology"**, CRC Press (2018).

[3] E.Y. Salih et al., "Rapid fabrication of NiO/porous Si film for ultra-violate photodetector: The effect of laser energy", *Microelectro. Eng.*, 258 (2022) 111758.

[4] M. Mahdi et al., "CdS nanocrystalline structured grown on porous silicon substrates via chemical bath deposition method", *Chalcogen. Lett.*, 9(1) (2012) 19-25.

[5] Q. Adfar, M. Aslam and S.S. Maktedar, "A Compendium of Metallic Inorganic Fillers' Properties and Applications Employed in Polymers", in **"Nanofillers"**, CRC Press (2023) pp. 25-68.

[6] F.J. Kadhim et al., "Photocatalytic activity of Ag-doped TiO_2 nanostructures synthesized by DC reactive magnetron co-sputtering technique", *Opt. Quantum Electron.*, 52(4) (2020) 1-9.

[7] J.A. Scholl, A.L. Koh and J.A. Dionne, "Quantum plasmon resonances of individual metallic nanoparticles", *Nature*, 483(7390) (2012) 421-427.

[8] A.B. Asha and R. Narain, "Nanomaterials properties", in **"Polymer Science and Nanotechnology"**, Elsevier (2020) pp. 343-359.

[9] M. Wilson, et al., **"Nanotechnology: basic science and emerging technologies"**, 1st ed., London (2002) pp. 23-26.

[10] K.W. Powers et al., "Characterization of the size, shape, and state of dispersion of nanoparticles for toxicological studies", *Nanotoxicology*, 1(1) (2007) 42-51.

[11] H. Bönnemann and R.M. Richards, "Nanoscopic metal particles− synthetic methods and potential applications", *Euro. J. Inorg. Chem.*, 2001(10) (2001) 2455-2480.

[12] A. Syafiuddin et al., "A review of silver nanoparticles: research trends, global consumption, synthesis, properties, and future challenges", *J. Chinese Chem. Soc.*, 64(7) (2017) 732-756.

[13] N. Kamarudheen, A. Sarkar and K.B. Rao, "Green synthesized nanoparticles from marine microbes and their biomedical applications", in **"Biological Synthesis of Nanoparticles and Their Applications"**, CRC Press (2019) pp. 65-84.

[14] M. Huston et al., "Green synthesis of nanomaterials", *Nanomater.*, 11(8) (2021) 2130.

[15] C. Richmonds and R.M. Sankaran, "Plasma-liquid electrochemistry: Rapid synthesis of colloidal metal nanoparticles by microplasma reduction of aqueous cations", *Appl. Phys. Lett.*, 93(13) (2008) 131501.

[16] Y.-T. Zhang, Y. Guo and T.-C. Ma, "Plasma catalytic synthesis of silver nanoparticles", *Chinese Phys. Lett.*, 28(10) (2011) 105201.

[17] E. Saion, E. Gharibshahi and K. Naghavi, "Size-controlled and optical properties of monodispersed silver nanoparticles synthesized

by the radiolytic reduction method", *Int. J. Mol. Sci.*, 14(4) (2013) 7880-7896.
[18] M. Vanaja and G. Annadurai, "Coleus aromaticus leaf extract mediated synthesis of silver nanoparticles and its bactericidal activity", *Appl. Nanosci.*, 3 (2013) 217-223.
[19] L.N. Nguyen et al., "Structural and optical sensing properties of nonthermal atmospheric plasma-synthesized polyethylene glycol-functionalized gold nanoparticles", *Nanomater.*, 11(7) (2021) 1678.
[20] J. Helmlinger et al., "On the crystallography of silver nanoparticles with different shapes", *Cryst. Growth Design*, 16(7) (2016) 3677-3687.
[21] S. Gómez-Graña et al., "Au@ Ag nanoparticles: Halides stabilize {100} facets", *J. Phys. Chem. Lett.*, 4(13) (2013) 2209-2216.
[22] J. Rodriguez-Loya, M. Lerma J.L. Gardea-Torresdey, "Dynamic Light Scattering and Its Application to Control Nanoparticle Aggregation in Colloidal Systems: A Review", *Micromachines*, 15(1) (2024) 24.
[23] M. Vinod and K. Gopchandran, "Ag@Au core–shell nanoparticles synthesized by pulsed laser ablation in water: effect of plasmon coupling and their SERS performance", *Spectrochimica Acta A: Mol. Biomol. Spectro.*, 149 (2015) 913-919.
[24] S.A. Khan et al., "Green synthesis of chromium oxide nanoparticles for antibacterial, antioxidant anticancer, and biocompatibility activities", *Int. J. Mol. Sci.*, 22(2) (2021) 502.
[25] E. Bulska and A. Ruszczyńska, "Analytical techniques for trace element determination", *Phys. Sci. Rev.*, 2(5) (2017) 20178002.

Table (1) XRD calculations of Ag nanoparticles at different concentrations

Concentration (M)	2θ (deg)	FWHM (deg)	Crystalline size (nm)	dhkl (Å) Practical	(hkl)
0.6	38.1	0.149	56.38	2.36	(111)
	44.27	0.20	42.86	2.04	(200)
	64.42	0.155	60.5	1.44	(220)
	77.47	0.17	59.88	1.23	(311)
0.8	38.1	0.152	55.27	2.36	(111)
	44.27	0.12	95.25	2.04	(200)
	64.42	0.226	41.52	1.44	(220)
	77.47	0.11	92.54	1.23	(311)
1	38.1	0.309	27.18	2.36	(111)
	44.27	0.146	90.24	2.04	(200)
	64.42	0.117	80.21	1.44	(220)
	77.47	0.195	52.20	1.23	(311)
1.2	38.1	0.43	19.53	2.36	(111)
	44.27	0.28	30.61	2.04	(200)
	64.42	0.56	16.76	1.44	(220)
	77.47	0.147	69.25	1.23	(311)
1.4	38.1	0.153	54.91	2.36	(111)
	44.27	0.19	45.12	2.04	(200)
	64.42	0.232	40.45	1.44	(220)
	77.47	0.16	63.62	1.23	(311)

Table (2) Elements concentration of the prepared samples

Sample No	Element (pph)										
	Nb	Mo	Rn	Rb	Pd	Ag	Cd	In	Sn	Sb	Te
0.6	<0.1	12.42	<0.1	<0.1	<0.1	748557.36	0.42	<0.1	8.39	0.79	147.06
0.8	<0.1	18.88	<0.1	<0.1	<0.1	391725.17	0.06	<0.1	1.66	0.58	0.00
1	<0.1	18.13	<0.1	<0.1	<0.1	2176512.81	0.24	<0.1	1.54	1.83	264.71
1.2	<0.1	19.36	<0.1	<0.1	<0.1	1691218.17	0.29	<0.1	8.80	0.36	117.06
1.4	<0.1	17.25	<0.1	<0.1	<0.1	1642063.22	0.25	<0.1	9.91	0.38	147.06

